

ELSEVIER
SCIENCE DIRECT

JOURNAL OF
ENVIRONMENTAL
CHEMICAL
ENGINEERING





ScienceDirect

Journal of Environmental Chemical Engineering

Supports *open access*

6.7

CiteScore

4.3

Impact Factor

Menu

Search in this journal

[Submit your article ↗](#)[Guide for authors ↗](#)

About the journal

[Aims and scope](#)[Editorial board](#)[Abstracting and indexing](#)

Editors

**Guilherme Luiz Dotto**

Federal University of Santa Maria, Department of Chemical Engineering, SANTA MARIA, Brazil

Adsorption/biosorption of contaminants from aqueous solutions, preparation and characterization of biomaterials and nanobiomaterials, wastewater treatment, wastes management, and reuse, drying of biomaterials, statistical optimization, experimental design, response surface methodology, linear and non-linear regression analysis

**Despo Fatta-Kassinou**

University of Cyprus Department of Civil and Environmental Engineering, Nicosia, Cyprus

Wastewater treatment, advanced oxidation processes, wastewater reuse, antimicrobial resistance, contaminants of emerging concern

**Yunho Lee**

Gwangju Institute of Science and Technology, Gwangju, Republic of Korea

Drinking water, disinfection, oxidation, ozone, advanced oxidation process, micropollutants, antibiotic resistance, water reuse

**Teik-Thye Lim**

Nanyang Technological University, Singapore, Singapore

Advanced Oxidation Processes; Environmental Catalysis; Industrial Wastewater Treatment; Environmental Nanomaterials; Resource Recovery

Associate Editors





Giovanni Palmisano

Khalifa University of Science & Technology, Department of Chemical Engineering, Abu Dhabi, United Arab Emirates

Photo(electro)catalysis applied to water treatment, Environmental remediation, H₂ generation, CO₂ reduction and selective oxidation; Self-cleaning surfaces



Vítor Vilar

University of Porto, Porto, Portugal

Environmental assessment and monitoring of surface waters, Environmental remediation technologies, Biological oxidation, Coagulation/flocculation, Adsorption/biosorption, Ion-exchange, Advanced oxidation processes, Electrochemical advanced oxidation processes, Ozonation, Membrane filtration, Wastewater resources recovery, Process integration & intensification, ,



Wen Zhang

New Jersey Institute of Technology, Department of Civil and Environmental Engineering, Newark, New Jersey, United States

Colloidal interfaces, nanomaterial characterization, environmental nanotechnology, reactive membranes



Xiwang Zhang

Monash University Department of Chemical Engineering, Clayton, Victoria, Australia

Membrane Synthesis, Membrane Process; 2D materials, Nanoporous Materials; Catalytic Oxidation and Resource Recovery.

Editorial Board Members



Diana Aga

University at Buffalo Department of Chemistry, Buffalo, New York, United States

Environmental Analysis, Emerging Contaminants, Persistent Organic Pollutants, Wastewater Treatment, Biodegradation, Antibiotic Resistance, Mass Spectrometry, Ecotoxicity



Taicheng An

Guangdong University of Technology - University Town Campus, Institute of Environmental Health and Pollution Control, Guangzhou, China

Fate and transport of micropollutants; Disinfection; Photocatalysis (heterogeneous); Air pollution control; Photocatalysis (air treatment)



Antonio Reinaldo Cestari

Federal University of Sergipe, Brazil

Sara J. Couperthwaite

Queensland University of Technology Faculty of Science and Engineering, Brisbane, Australia





A.J. Andrew J. Daugulis

Queen's University Department of Chemistry, Kingston, Ontario, Canada

Environmental Biotechnology, Bioresource Engineering, Cell Culture Engineering, and Industrial Bioprocessing



Ruey-an Doong

National Tsing Hua University, Institute of Analytical and Environmental Sciences, Hsinchu, Taiwan



Santi Esplugas

University of Barcelona, Barcelona, Spain

Advanced Oxidation Processes, Photocatalysis, Fenton, Ozonation, Wastewater treatment



Peiyong Hong

King Abdullah University of Science and Technology, Division of Biological and Environmental Science and Engineering, Thuwal, Saudi Arabia

Microbial contaminants, water quality, water reuse, wastewater, anaerobic biotechnologies



Hafiz M. N. Iqbal

Technological and Higher Education Institute of Monterrey, School of Engineering and Sciences, Monterrey, Mexico

Environmental Engineering, Bioengineering, Biomedical Engineering, Bioremediation, Emerging contaminants, Wastewater treatment, Biomaterials, Bio-catalysis, Enzymes, Enzyme-based pollutant degradation, Immobilization, Toxic heavy elements, Liquid and solid waste management, Valorization of agro-industrial wastes and by-products



Juan Lema

University of Santiago de Compostela, CRETUS Institute, Santiago de Compostela, Spain

Novel wastewater treatment processes; Anaerobic (co) Digestion; Removal of contaminants of emerging concern from wastewater and sludge;



Angela Yu-Chen Lin

National Taiwan University Graduate Institute of Environmental Engineering, Taipei, Taiwan

Emerging contaminants, Environmental photochemistry, Environmental chemistry and analysis, Transformation and risk of organic micropollutants, Water/wastewater treatment technology and reuse



Chao Liu

Clemson University, Department of Environmental Engineering and Earth Sciences, Anderson, South Carolina, United States

Drinking water quality, disinfection/oxidation, disinfection byproducts, contaminants of emerging concern, advanced water treatment





Célia Manaia

Catholic University of Portugal Faculty of Biotechnology, Porto, Portugal



In-Sik Nam

Pohang University of Science and Technology, Department of Chemical Engineering, Pohang, Korea, Republic of



Hyunwoong Park

Kyungpook National University, School of Energy Engineering, Daegu, South Korea

Roberto Parra Saldívar

Monterrey Institute of Technology and Higher Education, Monterrey, Mexico



Kaimin Shih

University of Hong Kong Department of Civil Engineering, Hong Kong, Hong Kong

Environmental Materials, Waste Engineering, Energy Materials, Waste-to-Resource, Wastewater Treatment



Maria Concetta Tomei

Water Research Institute National Research Council, Roma, Italy

Processes and Technologies for Urban and Industrial Wastewater Treatment, Modelling and Control of Biological Processes, Removal of Xenobiotic Compounds, Membrane bioreactors, Sludge Treatment, Soil Bioremediation



Zhiwei Wang

Tongji University School of Environmental Science and Engineering, Shanghai, China

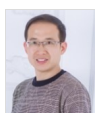
Wastewater treatment; Water reclamation; Membrane technology; Activated sludge treatment process; Resource recovery



Yeung-Sang Yun

Jeonbuk National University, School of Chemical Engineering, Jeonju, Korea, Republic of

Biosorbents and biosorption; Fate and degradation of emerging contaminants; Bio-inspired synthesis of nanomaterials; Boosting the natural purification process



Huabao Zheng

Zhejiang A and F University, Department of Environmental Science and Engineering, Hangzhou, China

Early Career Editorial Board



Oh Wen Da

Universiti Sains Malaysia, Pulau Pinang, Malaysia

Environmental catalysis, Advanced Oxidation Processes, Waste-to-Resources, Adsorption, Photocatalysis



Xiaoguang Duan

The University of Adelaide, Adelaide, Australia

Advanced Oxidation Processes, functional materials, nanocarbons, green catalysis, environmental nanotechnology



Patricia Garcia-Munoz

Polytechnic University of Madrid, Madrid, Spain

Advanced oxidation processes, Wastewater treatment, Photocatalysis, Fenton-related processes, Photocatalytic materials



Yuxiong Huang

Tsinghua-Berkeley Shenzhen Institute, Shenzhen, China

Environmental Nanotechnology, Water Treatment, Environmental Analytical Chemistry, Emerging Contaminants, Surface and Interfacial Engineering



Popi Karaolia

University of Cyprus, Lefkosia, Cyprus

Antibiotic resistance, Advanced Oxidation Processes, Wastewater treatment, Membrane Bioreactor, Disinfection



Choonsoo Kim

Kongju National University, Gongju, Korea, Republic of

Electrochemical Water treatment, Electrochemical Advanced Oxidation Process (EAOP), Electrochemical Ion Separation (EIONS), Capacitive Deionization (CDI), Resource Recovery



Francisca Moreira

University of Porto, Porto, Portugal

Wastewater treatment, Process integration and intensification, Organic synthesis, Wastewater resources recovery, Electrochemical advanced oxidation processes



Francesco Parrino

University of Trento Department of Industrial Engineering, Povo, Italy

Photocatalysis, Ozonation, Plasma, Process Intensification, Advanced Oxidation Processes, Green Chemistry, Photocatalytic Syntheses, Kinetic Modelling, Photoactive Materials, Environmental Chemistry



Hugo Olvera Vargas

National Autonomous University of Mexico, Mexico City, Mexico

Environmental electrochemistry, Electrochemical advanced oxidation processes, Wastewater treatment and resource recovery, Photoelectrocatalysis, Environmental analysis and emerging contaminants



Dawei Wang

Hohai University, Nanjing, China

Nanomaterials, Photocatalysis, Advanced Oxidation Process, Emerging Contaminants, Wastewater

All members of the Editorial Board have identified their affiliated institutions or organizations, along with the corresponding country or geographic region. Elsevier remains neutral with regard to any jurisdictional claims.

ISSN: 2213-3437

Copyright © 2021 Elsevier Ltd. All rights reserved



Copyright © 2021 Elsevier B.V. or its licensors or contributors.
ScienceDirect® is a registered trademark of Elsevier B.V.



Volume 9, Issue 2

In progress (April 2021)

This issue is in progress but contains articles that are final and fully citable.

[< Previous vol/issue](#)[Next vol/issue >](#)

Receive an update when the latest issues in this journal are published

[Sign in to set up alerts](#)

Research Articles

Research article Abstract onlySimbang Darah (*Iresine herbstii*) extract mediated hydrothermal method in the synthesis of zinc ferrite spinel nanoparticles used for photocatalysis and antibacterial applications

Rahmayeni, Rike Febrialita, Yeni Stiadi, Yulia Eka Putri, ... Zulhadjri

Article 105140

[Purchase PDF](#) [Article preview](#)Research article Abstract onlyStatistical optimization of levulinic acid and formic acid production from lipid-extracted residue of *Chlorella vulgaris*

Gwi-Taek Jeong, Sung-Koo Kim

Article 105142

[Purchase PDF](#) [Article preview](#)Research article Abstract onlyNiMn₂O₄ sphere catalyst for the selective catalytic reduction of NO by NH₃: Insight into the enhanced activity via solvothermal method

Jiangning Liu, Xu Wu, Benhui Hou, Yali Du, ... Baoshuan Yang

Article 105152



Article 105154

[Purchase PDF](#) Article preview Research article Abstract only**On the hydrothermal-enhanced synthesis of highly selective Mo₂C catalysts to fully deoxygenated products in the guaiacol HDO reaction**

E. Ochoa, D. Torres, J.L. Pinilla, I. Suelves

Article 105146

[Purchase PDF](#) Article preview Research article Abstract only**Removal of benzophenone aerosols by a rice straw-based activated carbon filter combined with a negative air ionizer**

Ming-Hsuan Tsai, Abiyu Kerebo Berekute, Yu Wei Tsai, Kun-Yi Lin, Kuo-Pin Yu

Article 105141

[Purchase PDF](#) Article preview Research article Abstract only**Preparation and characterization of magnetic photocatalyst from the banded iron formation for effective photodegradation of methylene blue under UV and visible illumination**

Moustafa M.S. Sanad, Mohsen M. Farahat, Soliman I. El-Hout, Said M. El-Sheikh

Article 105127

[Purchase PDF](#) Article preview Research article Abstract only**CO₂ adsorption investigation by statistical physics: Thermodynamic analysis for cooling cycle application**

Wouroud Sghaier, Yosra Ben Torkia, Mohamed Bouzid, Abdelmottaleb Ben Lamine

Article 105108

[Purchase PDF](#) Article preview Research article Abstract only**Activated carbon from macauba endocarp (*Acrocomia aculeate*) for removal of atrazine: Experimental and theoretical investigation using descriptors based on DFT**

Wedja Timóteo Vieira, Mozart Daltro Bispo, Samara de Melo Farias, Arthur da Silva Vasconcelos de Almeida, ... Tatiane Luciano Balliano

Article 105155

[Purchase PDF](#) Article preview Research article Abstract only**Engineering of oxygen vacancy as defect sites in silicates for removal of diverse organic pollutants and enhanced aromatic alcohol oxidation**

Debashrita Sarkar, Khushboo S. Paliwal, Sagar Ganguli, Athma E. Praveen, ... Venkataramanan Mahalingam

Article 105134

[Purchase PDF](#) Article preview

[Purchase PDF](#) Article preview Research article Abstract only**Environmentally friendly magnetic chitosan nano-biocomposite for Cu(II) ions adsorption and magnetic nano-fluid hyperthermia: CCD-RSM design**

Elham Cheraghipour, Mahmoud Pakshir

Article 104883

[Purchase PDF](#) Article preview Research article Abstract only**Peroxydisulfate activation process on copper oxide: Cu(III) as the predominant selective intermediate oxidant for phenol and waterborne antibiotics removal**

Chan Li, Vincent Goetz, Serge Chiron

Article 105145

[Purchase PDF](#) Article preview

Short Communications

Short communication Abstract only**The presence of low fouling-causing bacteria can lead to decreased membrane fouling potentials of mixed cultures**

Naga Raju Maddela, Ronald Oswaldo Villamar Torres

Article 105131

[Purchase PDF](#) Article preview

Special Issue on Advanced Oxidation Processes for Water and Wastewater Treatment

Research article Abstract only**Cytotoxic effects of silver nanoparticles on *Ruellia tuberosa*: Photocatalytic degradation properties against crystal violet and coomassie brilliant blue**

Vasantharaj Seerangaraj, Selvam Sathiyavimal, Sripriya Nannu Shankar, Jaya Ganesh Thiruvengadam Nandagopal, ... Arivalagan Pugazhendhi

Article 105088

[Purchase PDF](#) Article preview

Journal of Environmental Chemical Engineering

Supports *open access*



6.7

4.

CiteScore
 Ir



Copyright © 2021 Elsevier B.V. or its licensors or contributors.
ScienceDirect® is a registered trademark of Elsevier B.V.



Simbang Darah (*Iresine herbstii*) extract mediated hydrothermal method in the synthesis of zinc ferrite spinel nanoparticles used for photocatalysis and antibacterial applications

Rahmayeni^{a,*}, Rike Febrialita^a, Yeni Stiadi^a, Yulia Eka Putri^a, Nofrijon Sofyan^b, Zulhadjri^a

^a Department of Chemistry, Faculty of Mathematics and Natural Sciences, Universitas Andalas, Kampus Limau Manis, Padang 25163, Indonesia

^b Department of Metallurgical and Materials Engineering, Faculty of Engineering, Universitas Indonesia, Kampus Baru UI-Depok, 16424, Indonesia

ARTICLE INFO

Editor: Dr. G.L. Dotto

Keywords:

ZnFe₂O₄ nanoparticles
Hydrothermal
Iresine herbstii
Direct red 81
Antibacterial

ABSTRACT

This paper reports the use of Simbang Darah (*Iresine herbstii*) leaf extract to synthesize ZnFe₂O₄ spinel ferrite nanoparticles via hydrothermal method. Biochemical compounds in Simbang Darah leaf extract act as a capping agent and a stabilizer to form nanostructures. XRD patterns and FTIR spectrums confirm the formation of the cubic spinel crystal structure of ZnFe₂O₄ nanoparticles. SEM and TEM characterization revealed that ZnFe₂O₄ spinel ferrite morphology has a uniform spherical shape in nanoscale. EDX results showed that the compositional mass ratios were relevant as expected from the synthesis. ZnFe₂O₄ nanoparticles have an absorption edge in the visible region with Eg values within the range 2.05–2.11 eV in the DRS UV–Vis analysis. The as-prepared samples exhibit paramagnetic behavior according to the magnetic hysteresis curve. ZnFe₂O₄ nanoparticles were proven effective in direct red 81 dye photodegradation (99.66%) after exposure to solar light irradiation for two hours. On top of that, ZnFe₂O₄ nanoparticle exhibited antibacterial activity against *S. aureus* and *E. coli*.

1. Introduction

Zinc ferrite (ZnFe₂O₄) is an important magnetic material that has attracted significant interest due to its unique optical, magnetic, and electrical properties. It has a normal spinel phase where Zn²⁺ ions occupy the tetrahedral site, and Fe³⁺ ions occupy the octahedral site. In nanoscale, the changes of ZnFe₂O₄ structure into mixed spinel can increase its magnetic properties to become superparamagnetic [1,2]. Zinc ferrite has been widely used in many fields such as biomedicine [3], the production of battery anodes [4], gas sensors [5,6], planar drug delivery [7], besides acting as antibacterial agent [8], photocatalysts, and absorbent material [9,10]. It can be manufactured via various techniques such as co-precipitation route [11], one step and multistep hydrothermal method [12,13], solvothermal method [10], combustion route [14], solution combustion reaction [6], thermal method using reducing and capping agents [15], and soft chemical route [16]. Each method has its advantages and disadvantages such as simplicity, convenience, temperature, and hazardous chemicals usage.

Many researchers are currently focused on using natural substances derived from plants or microorganism to synthesize functional materials. This approach can replace hazardous chemicals and offer an

environmentally friendly synthesis [17]. In addition, the utilization of several plant extracts as stabilizers in the biosynthesis of ferrite material with nanostructures has been proven to be environmentally friendly, easy to obtain, low-cost, and non-toxic [18].

In recent years, there have been many reports of the green synthesis of ZnFe₂O₄ compound by different methods. For instance, Kombaiah et al. [19] synthesized ZnFe₂O₄ using *Hibiscus rosa-sinensis* extract as a reducing and stabilizer agent via conventional and microwave combustion methods. Meanwhile, Patil et al. [14] used sugarcane juice as fuel in ZnFe₂O₄ synthesis via combustion method. Additionally, Matinise et al. [20] utilized *Moringa oleifera* extract as chelating and reducing agents in the synthesis of ZnFe₂O₄. Furthermore, *Limonia acidissima* juice was used as fuel in the synthesis of ZnFe₂O₄ using microwave by Madhukara Naik et al. [21]. Moreover, Sriramulu et al. [17] used *Aegle marmelos* leaves extract in the synthesis of ZnFe₂O₄. The biosynthesis of zinc ferrite produced small particles with a homogeneous, smooth, and stable structure [18].

Simbang Darah (*Iresine herbstii*) is a family of *Amaranthaceae* with various leaf colors ranging from purple or dark purple to green (Fig. 1). Its leaves have been used as a traditional remedy for eczema and acne scars for humans. Besides, Simbang Darah leaves are boiled in water and

* Corresponding author.

E-mail address: rahmayenni@sci.unand.ac.id (Rahmayeni).

<https://doi.org/10.1016/j.jece.2021.105140>

Received 24 October 2020; Received in revised form 18 January 2021; Accepted 27 January 2021

Available online 29 January 2021

2213-3437/© 2021 Elsevier Ltd. All rights reserved.



Fig. 1. Simbang Darah (*Iresine herbstii*) leaves.

used as an antipyretic and tonic to treat anemia. In the biomedical field, Simbang Darah has been used as an anti-cancer and antimicrobial agent [22,23]. Simbang Darah contains several compounds including 3', 4', 7-trihydroxy-6-methoxy flavone, N-feruloyltyramine, glycinebetaine and trigonelline, betacyanin acylate-amaranthine, isoamaranthine, iresin I, isoiresin I (= iresin II), iresinin III and iresinin IV [24]. In the latest research, this plant was found to contain isoflavone compounds 2', 2, 5-trimethoxy-6,7-methylenedioxyisoflavone and tlatlancuayin isoflavones (2', 5-dimethoxy-6,7-methylenedioxyisoflavone) [25]. Several advantages of using Simbang Darah leaves include easy to obtain, easy to extract, and economical. As of today, there have been no reports of ZnFe₂O₄ hydrothermal synthesis using Simbang Darah leaf extract.

In this study, a green synthesis approach was used to synthesize ZnFe₂O₄ magnetic material via the hydrothermal method using Simbang Darah extract as a capping and a stabilizer agent. The obtained ZnFe₂O₄ nanoparticles were characterized using several instruments to analyze the crystal structure and crystallite size, morphology, magnetic properties, optical properties, binding energy, and interatomic interactions in their spinel structures. The photocatalytic activity of ZnFe₂O₄ was evaluated on the degradation of direct red 81 dyes under natural sunlight. Direct red 81 with molecular formula C₂₉H₁₉N₅Na₂O₈S₂ is one of the synthetic dyes in the textile industry and has been known for its carcinogenic nature and toxicity towards animals and humans [26,27]. Furthermore, the antibacterial activity of ZnFe₂O₄ was also tested against pathogenic bacteria found in wastewater, i.e., *S. aureus* and *E. coli*.

2. Materials and methods

2.1. Materials

Zn(NO₃)₂·4H₂O (Sigma-Aldrich) and Fe(NO₃)₃·9H₂O (Sigma-Aldrich) were used as precursors without further treatment. NaOH (Merck) was used as a mineralizer, with Nutrient agar, and distilled water. Direct red 81 dye was obtained from the local textile factory. Meanwhile, Simbang Darah (*Iresine herbstii*) leaves were obtained from Alahan Panjang, West Sumatra, Indonesia. The pathogenic bacteria were obtained from the Microbiology Laboratory, Faculty of Agriculture, Universitas Andalas. All solutions were prepared using deionized water.

2.2. Extract preparation

Simbang Darah leaves (Fig. 1.) were separated from the stems, washed with distilled water, and dried in a closed room (25–28 °C) for ten days. Then, the dried leaves were blended into fine powder form. A total of 5 g of Simbang Darah leaf powder was added to 100 mL of distilled water and heated for 2 h at 58 °C under agitation at 300 rpm. After that, the extract was filtered and stored in a refrigerator momentarily before synthesizing zinc ferrite nanoparticles.

2.3. Synthesis of ZnFe₂O₄ nanoparticles

The ZnFe₂O₄ nanoparticles were synthesized via the hydrothermal method [28] using Simbang Darah leaf extract as a capping agent. A total of 1.49 g Zn(NO₃)₂·4H₂O and 4.04 g Fe(NO₃)₃·9H₂O were mixed in 50 mL Simbang Darah extract solution. The concentration of Simbang Darah solution was varied by adding 1, 3, and 5 mL of concentrated extract in 50 mL of solution. The mixture was stirred at 500 rpm for 1 h before adding 4 M sodium hydroxide (NaOH) to the mixture until pH of 12 was achieved. The stirring was continued for another 2 h. Later, the suspension was poured into an autoclave tube and heated at 180 °C for 3 h. The resulted precipitation was filtered, washed several times using distilled water until the pH 7 was achieved, and then heated in an oven at 110 °C for 4 h. The obtained ZnFe₂O₄ powders were labeled as ZnE₁N, ZnE₃N, and ZnE₅N, respectively. In order to investigate the effect of temperature on the structure formation of ferrite, the samples were calcined at 500 °C for 2 h. After that, the calcined ferrite powders were labeled as ZnE₁NK, ZnE₃NK, and ZnE₅NK for 1, 3, and 5 mL extracts, respectively.

2.4. Material characterization

The phase composition and crystalline structure of zinc ferrite nanocrystals were studied using X-ray diffraction (PANalytical X'pert Pro Multipurpose Diffractometer) with Cu-Kα radiation (λ = 1.5406 Å) at 2θ ranging from 10° to 90°. The structural parameters were refined using the Le Bail method available in RIETICA software [29]. Then, the average crystallite size was calculated using the standard Scherer formula [18]. Surface morphology and chemical composition of ferrite were examined using a scanning electron microscope (SEM, JEOL JSM-6360LA) embedded with energy-dispersive X-ray spectroscopy (EDS). Detailed morphology of the samples was investigated using a transmission electron microscope (TEM, JEM-1400). High-resolution transmission electron microscopy (FEI, Technai G2, F30) was employed to probe the microstructure, particle size distribution, and high-resolution imaging of zinc ferrite. The binding energy of zinc ferrite was determined by X-ray photoelectron spectroscopy (XPS ULVAC-PHI Quantera SXM). The UV-Vis spectrophotometer analyzed the photo-absorption measurement of ferrites (Shimadzu UV-Vis 2450). The samples' magnetic properties were investigated using a vibrating sample magnetometer (VSM OXFORD 1.2H). FTIR spectra were recorded using a Nicolet IR200FT-IR spectrometer using KBr pellet technique. The adsorption-desorption isotherms were conducted using a surface area and pore size analyzer (BET, Quantachrome Nova 2000 E).

2.5. Determination of zinc ferrite photocatalytic activity

The photocatalytic activity of the synthesized ZnFe₂O₄ nanoparticles was determined under solar light irradiation for direct red 81 dye adapted from [28]. ZnFe₂O₄ catalyst in powder form was added to a petri dish containing 20 mL of 35 mg L⁻¹ direct red 81 solutions (pH = 6) and stored in a dark box for 30 min to investigate the adsorption process. The mixtures were then exposed for 2 h under natural solar light irradiation. Furthermore, the liquid was separated from the catalyst, and supernatant absorption was measured at a wavelength of 530 nm using a UV-visible spectrophotometer. The degradation percentage was calculated with % Deg. = (A₀ - A_t)/A₀ × 100% using the absorbance of direct red 81, where A₀ and A_t are the initial absorbance and the absorbance at time t, respectively. Moreover, the same experiments were performed with the ZnE₁N, ZnE₃N, ZnE₅N, ZnE₁NK, ZnE₃NK, and ZnE₅NK samples. Two samples with the best activity were further tested for several parameters related to photocatalytic activity, i. e., radiation duration (0.5, 1, 1.5, and 2 h) and dye concentration (25, 30, 35, 40, and 45 mg L⁻¹). The samples were retested in the same manner to investigate their durability and stability against repeated use. Prior to retesting, the used samples were rinsed with distilled water and

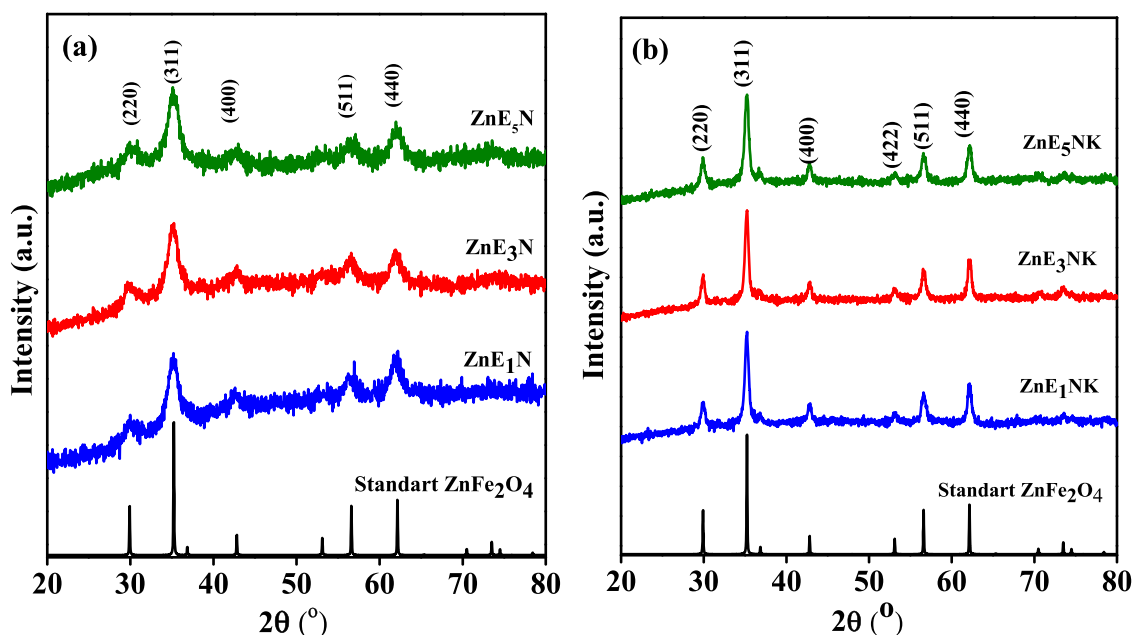


Fig. 2. XRD patterns of ZnFe_2O_4 before (a) and after calcination (b) at 500°C prepared using Simbang Darah leaf extracts at various concentrations.

later heated in an oven at 110°C for 2 h for activation.

2.6. Determination of zinc ferrite antibacterial activity

The antibacterial activities of the samples were screened using two pathogenic bacteria, *S. aureus* and *E. coli*, according to [30,31]. Nutrient agar (NA) was used as a growth media to observe nanoparticles' bactericidal activity in-vitro. Firstly, NA was autoclaved at 120°C for 20 min and then cooled to 45°C . Petri dishes for the antibacterial assay were also sterilized in an autoclave. Meanwhile, the bacteria were subcultured in 5 mL of sterile distilled water overnight. A total of 0.1 mL of the bacterial suspension was added to 20 mL of NA media and homogenized. Then, the NA media containing the bacteria was poured into a sterile petri dish and allowed to solidify. The ZnFe_2O_4 samples were inserted into the wells that had been prepared in the NA media. Amoxicillin was used as a positive control and water as a negative control in this experiment. The inhibition zones of the samples were measured after incubation at 37°C for 24 h.

3. Results and discussion

3.1. XRD powder analysis

The XRD patterns of the ZnFe_2O_4 samples synthesized via the hydrothermal method in the presence of Simbang Darah leaf extract before and after calcination are shown in Fig. 2. XRD patterns of ZnE_1N , ZnE_3N , and ZnE_5N are shown in Fig. 2a. All XRD peaks have been identified and confirmed to be single-phase ZnFe_2O_4 indexed to $Fd\bar{3}m$ cubic crystal structure (ICSD-158837). The crystallite sizes calculated using the Debye-Scherrer's formula are 7.2, 6.8, and 6.0 nm for ZnE_1N , ZnE_3N , and ZnE_5N , respectively. The decrease in crystallite size can also be observed visually through the broadening of the diffraction peaks.

Similarly, XRD analysis was also carried out on calcined ZnE_1NK , ZnE_3NK , and ZnE_5NK samples, as shown in Fig. 2b. The XRD patterns were similar to that of Fig. 2a, but with sharper and well-resolved peaks. The crystallite sizes of the ZnE_1NK , ZnE_3NK , and ZnE_5NK samples increase with the calcination process recording 15.8, 16.9, and 14.4 nm, respectively. These results indicated that the calcination accelerates the crystal's grain growth due to the coalescing of many crystallites of the same orientation, forming a large grain with a particular orientation

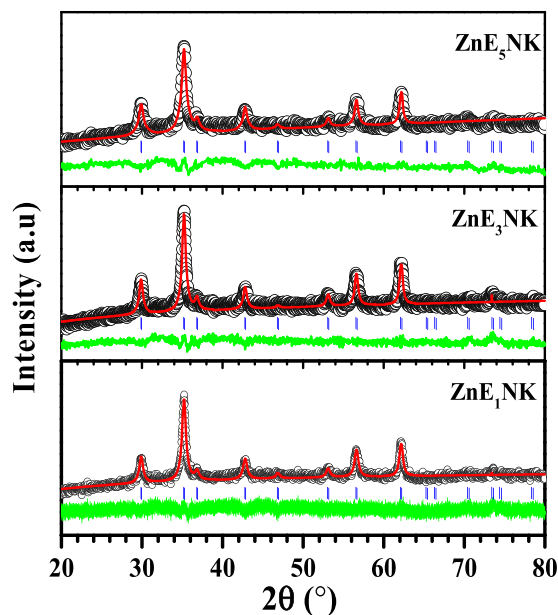


Fig. 3. Rietveld refinement patterns of ZnFe_2O_4 after calcination at 500°C .

[32]. Both XRD pattern and crystallite size of the samples suggested that the Simbang Darah leaf extracts at varying concentrations influenced the formation of ZnFe_2O_4 ferrite material with spinel structure. The

Table 1
Refined structural parameters of single-phase ZnFe_2O_4 samples after calcination.

Parameter	ZnE_1NK	ZnE_3NK	ZnE_5NK
Space group	$Fd\bar{3}m$	$Fd\bar{3}m$	$Fd\bar{3}m$
Crystal class	Cubic	Cubic	Cubic
$a = b = c$ (Å)	8.4499	8.4487	8.4458
V (Å ³)	603.33	603.07	602.45
Z	8	8	8
R_p (%)	2.12	2.65	2.16
R_{wp} (%)	2.68	3.15	2.78
χ^2	1.41	3.91	1.59

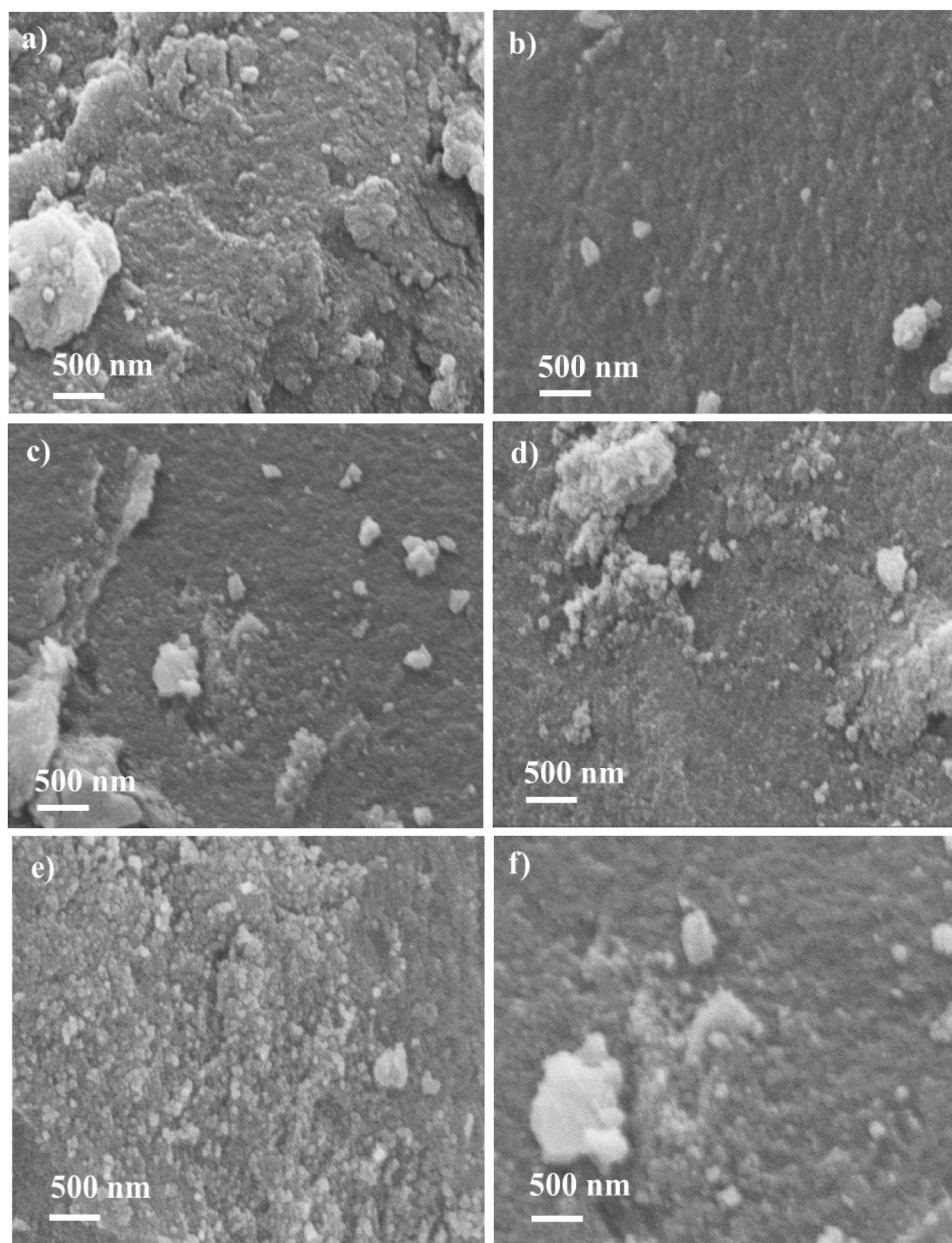


Fig. 4. Secondary electron images of (a) ZnE_1N , (b) ZnE_3N , (c) ZnE_5N , (d) ZnE_1NK , (e) ZnE_3NK , and (f) ZnE_5NK .

decreased in crystallite size with the increase of the extract concentration revealed that the secondary metabolites of the Simbang Darah could control the crystal growth.

The structural parameters of the nanoparticles were investigated using the Le Bail refinement method available in the RIETICA program. Initial parameters for the refinement were used from the cubic $Fd\bar{3}m$ ZnFe_2O_4 (ICSD-158837). Fig. 3 shows Le Bail profile to the XRD patterns of ZnFe_2O_4 samples after calcination. All XRD peaks were well-fitted with the Bragg reflections in the $Fd\bar{3}m$ space group, confirming that all samples were single-phase [33]. The refined structural parameters are given in Table 1. Besides, the lattices parameters and cell volume were relatively constant for all samples, demonstrating that the concentration of extract did not change the structure of ZnFe_2O_4 .

3.2. SEM analysis

The morphology of synthesized ZnFe_2O_4 nanoparticles was analyzed using SEM instrument. Fig. 4 shows that all secondary electron images of

the samples have spherical shapes morphology with some clusters and aggregated nanoparticles. Fig. 4(a-c) demonstrates the morphology of ZnE_1N , ZnE_3N , and ZnE_5N particles. The samples have more distinct homogeneity spherical morphologies with smaller particle size and less aggregation. Meanwhile, the ZnE_1NK , ZnE_3NK , and ZnE_5NK particles also exhibited spherical morphologies with slightly larger particle size and agglomerations.

Generally, the agglomerating tendency is found in ferrite nanoparticles due to its high surface energy, magnetic nanomaterials [34]. The estimated particle size distribution ranged from 10 to 40 nm for ZnE_1N , ZnE_3N , and ZnE_5N , whereas for ZnE_1NK , ZnE_3NK , and ZnE_5NK is in the range of 20–80 nm. These results are in agreement with [35] which have nanoparticle diameters ranging from 10 nm to 50 nm but smaller and homogeneous than that obtained by [34]. The homogeneous shape and the small size of ferrite particles are very beneficial for their photocatalytic activity applications. Smaller grain size has a larger surface area, leading to better interaction with the dye molecules in the liquid medium. Thus, it can be concluded that the morphology of the

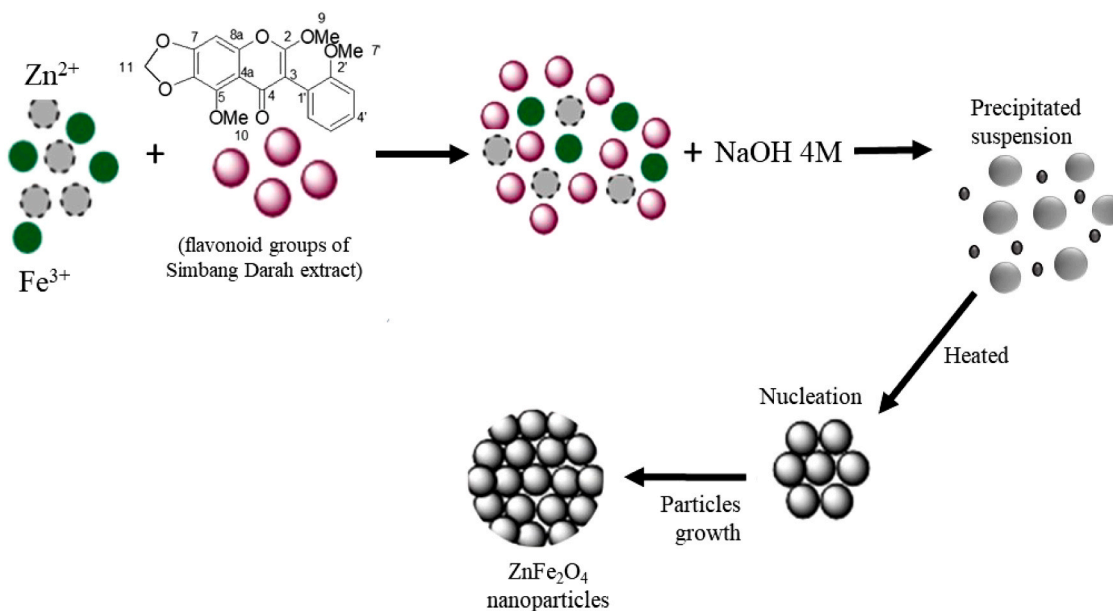


Fig. 5. Schematic diagram of the proposed formation mechanism of ZnFe₂O₄ nanoparticles in the presence of Simbang Darah extracts as a capping agent.

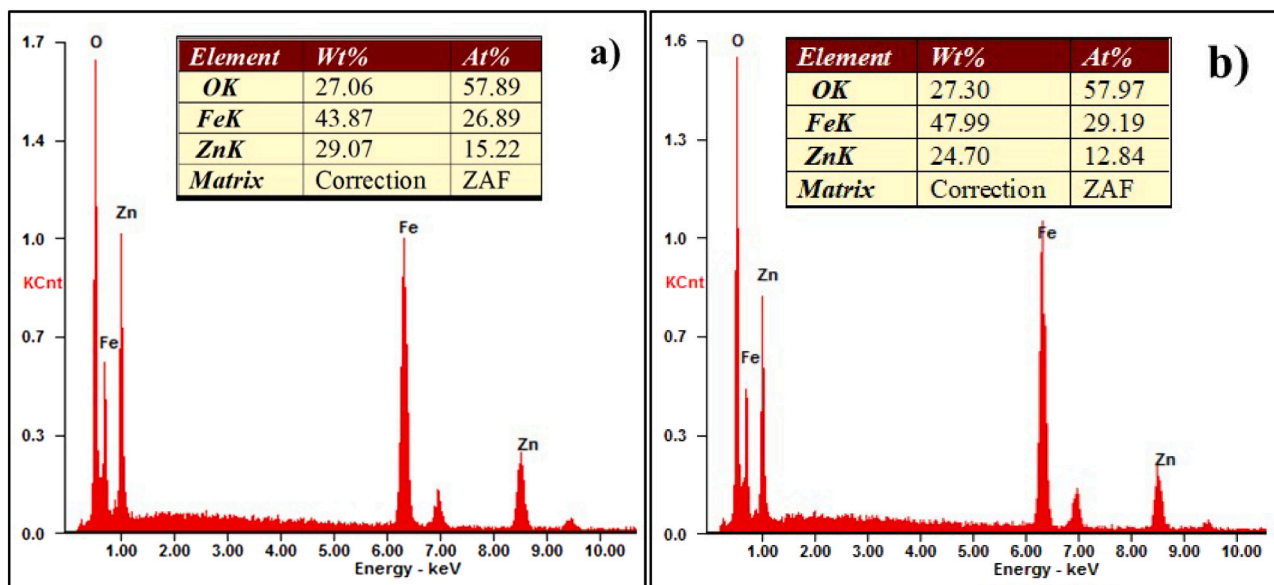


Fig. 6. EDX spectrum of ZnE₁N (a) and ZnE₁NK (b).

materials is affected by Simbang Darah leaf extract concentration and the calcination process. The proposed mechanism towards the formation of ZnFe₂O₄ nanoparticles in the presence of Simbang Darah extracts as the capping agent is presented in Fig. 5.

3.3. EDX analysis

The composition of the elements in the ferrites obtained from EDX is shown in Fig. 6. The EDX spectrum shows the presence of Zn, Fe, and O elements only in both samples. The weight percentages of Zn, Fe, and O elements in ZnE₁N particles were 27.06%, 43.87%, and 29.07%, respectively, whereas ZnE₁NK were 24.70%, 47.99%, and 27.3%, respectively. Fe and Zn's percentage in the samples suggested that the ratio of Fe: Zn atoms was close to 2:1, confirming the formation of ZnFe₂O₄ ferrite spinel structure. As shown in the spectra, the peaks are ascribed to the photocatalyst elements, and no other elements are found.

It indicated the high purity of ZnFe₂O₄ samples.

3.4. TEM analysis

Detailed morphology and structure of ZnFe₂O₄ were investigated using TEM (Fig. 7). Fig. 7(a-b) show the TEM photographs of ZnE₁N that revealed particle-like shape with a uniform size distribution in the range of 6–8 nm. This finding correlates to the data obtained using XRD. Fig. 7b inset shows the particles size distribution and particle count histogram, resulting in more particles having a grain of 6 nm. The selected area electron diffraction (SAED) pattern (Fig. 7d) shows the spot type pattern as an indication of good crystallinity. The distinct lattice fringes were evident in the high-resolution TEM (HRTEM) image (Fig. 7c) suggesting that ZnFe₂O₄ is good crystalline in nature. The crystal planes were also clearly visible from the images, and the lattice plane fringes were used to calculate the d-spacing values. The d-spacing

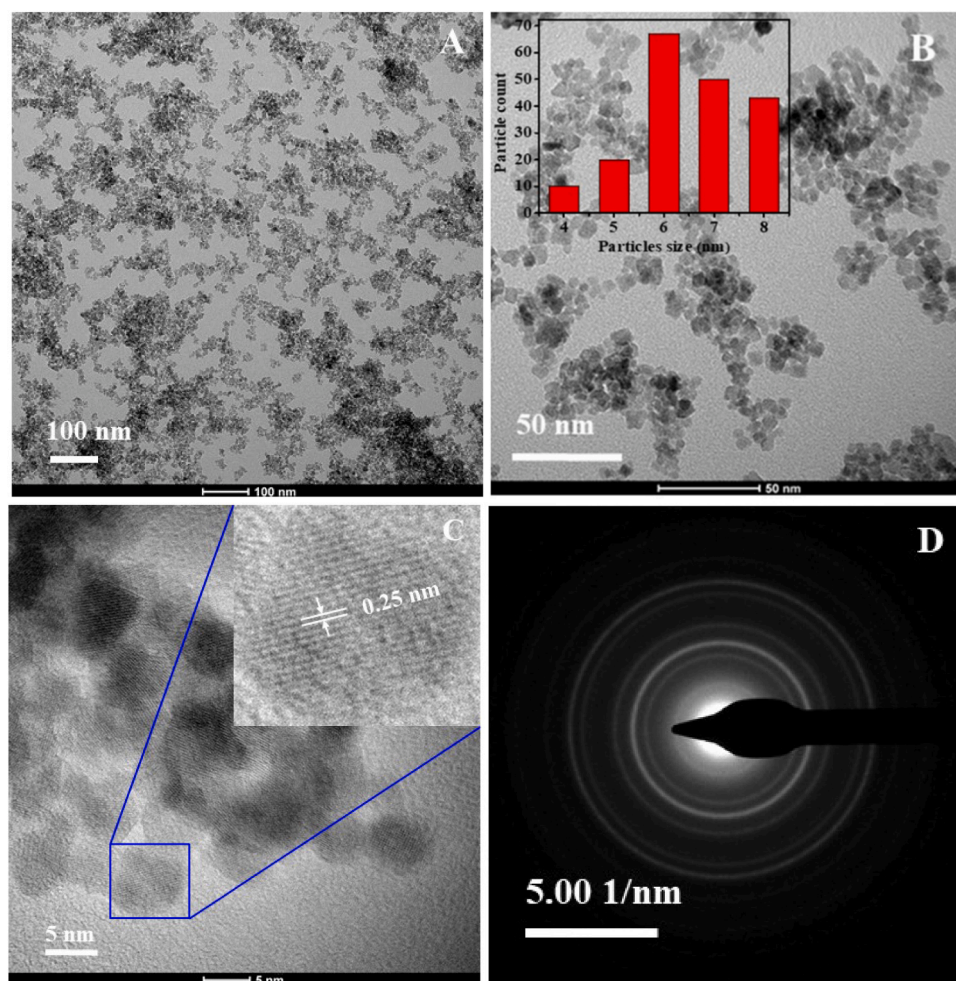


Fig. 7. TEM micrograph (a-b), HRTEM micrograph (c), and SAED pattern of ZnE₁N (d). Insert in b) is the histogram of particles distribution.

of 0.25 nm corresponded to the (311) crystal plane of ZnFe₂O₄. This value aligned with the value of 2.5 Å, calculated using the Bragg's equation using the XRD result of a representative ZnFe₂O₄ [36]. This finding is further supported by the presence of intense rings that were well resolved in the SAED pattern.

3.5. XPS analysis

The X-ray photoelectron spectroscopy (XPS) measurement was used to analyze the chemical state of the elements in the ZnE₁N spinel ferrite. The results are displayed in Fig. 8(a and b). From the full spectrum of ZnFe₂O₄ in Fig. 8a, it can be observed that the sample consisted of Zn, Fe, O, and C binding energies with no other impurities. In Fig. 8b, the binding energies of Zn 2p_{1/2} and Zn 2p_{3/2} are 1045 eV and 1022 eV, respectively. Compared with the standard spectrum, these energies are suitable for Zn²⁺ [37]. The spectrum of Fe shows two peaks located at 708, and 720 eV for 2p_{3/2} and 2p_{1/2} corresponding to Fe³⁺ ion in the spinel ferrite. The presence peak of C 1s at 284.8 eV was introduced during the reaction process or exogenously substances during testing.

3.6. UV-Vis DRS analysis

The optical properties of ZnFe₂O₄ nanoparticles synthesized via the hydrothermal method and further calcined at 500 °C were investigated using UV-Visible reflectance spectroscopy. The samples' UV-DRS spectrum shows a strong absorption band at the visible light area (Fig. 8c). The band gap energy of the ZnFe₂O₄ nanoparticles was evaluated from the spectrum using the Kubelka-Munk model [38]. For the band gap

determination, a graph (a Taucplot) is plotted between $[F(R)h\nu]^2$ and energy (eV), and the intercept is the band gap energy as shown in Fig. 8d. The band gap energy for all samples is shown in Table 1. From Table 1, it can be seen that the band gap energies are in the range 2.05–2.11 eV, which are in good agreement with the previously reported values [14] using sugarcane juice extract and another report [39] using *Hibiscus rosa sinensis* extract. The band gaps of the synthesized ZnFe₂O₄ are in the range of 2.05–2.11 eV, which are expected to reduce the possibility of recombination of electrons from the conduction band to valence band and thus improve the catalytic activity. The band gap variation depends on various factors such as crystallinity, crystallite size, structural parameters, lattice strain, and the presence of defects or impurities [8,38]. In our case, the variation of band gap correlates with the crystallinity and crystallite size [21]. The observed blue shift in Fig. 9a is mainly attributed to the smaller crystallite size of the samples.

3.7. VSM analysis

The magnetization curves of ZnFe₂O₄ and the value of magnetic saturation (*M_s*), magnetic remanent (*M_r*) and coercive field (*H_c*) before and after calcination are shown in Fig. 9 and Table 2. The hysteresis curve shows that all ZnFe₂O₄ un-calcined samples have paramagnetic behavior.

The *M_s* value for the un-calcined samples increased (1.69, 1.74, and 2.08 emu/g) as the crystallite size decrease. Similarly, *M_s* increased when the sample was calcined at 500 °C because of the arrangement of atoms and dipoles in the crystal lattice as the temperature is raised. It was observed that all *M_s* values of the synthesized samples are smaller

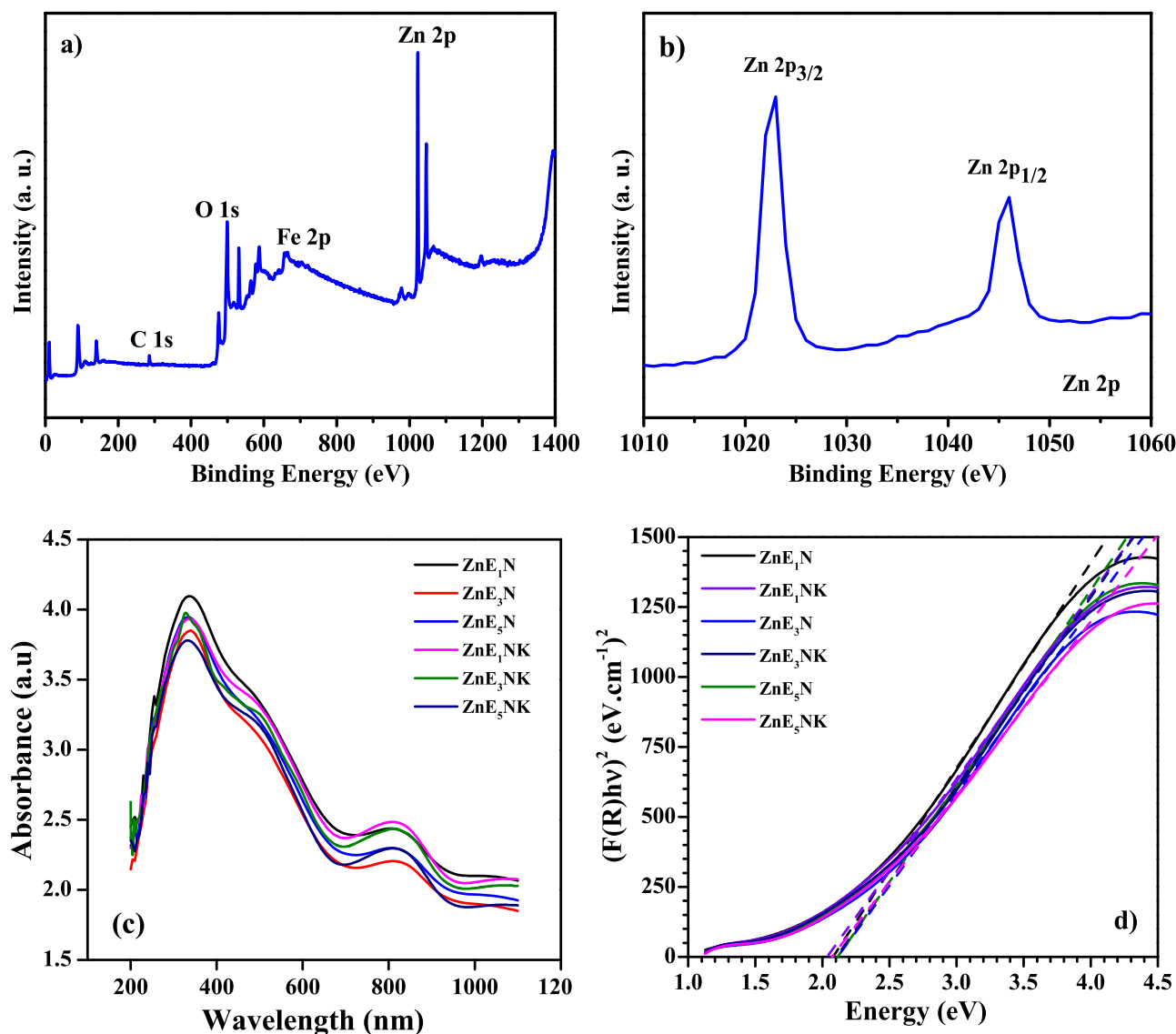


Fig. 8. XPS spectrum of ZnE₁N (a and b), DRS UV-Vis spectrum (c) and band gap energy (d) of samples.

than those obtained by [38]. Moreover, M_s , M_r , and H_c values obtained in this experiment indicated that the Simbang Darah leaf extract concentrations affect the crystallinity and magnetic properties of ZnFe₂O₄. Furthermore, the calcined samples of ZnE₁NK, ZnE₃NK, were paramagnetic, while ZnE₅NK exhibited superparamagnetic behavior. The calcination process of ZnFe₂O₄ will change ferrite behavior from paramagnetic to superparamagnetic. The presence of magnetic properties confirmed the efficacy of zinc ferrite as a photocatalyst because it can be separated from the liquid using an external magnetic field. Thus, these materials can be used for subsequent photocatalytic processes.

3.8. FTIR analysis

The structure of ZnFe₂O₄ ferrite nanoparticles before (a) and after calcination (b) was further studied by characterizing the samples using FTIR as shown in Fig. 10. Two prominent absorption bands of the spinel ferrite were observed in all spectra of the samples ranging from 300 to 600 cm⁻¹ indicating the spinel ferrite of ZnFe₂O₄. Apart from that, strong absorbance bands around 540–580 cm⁻¹ corresponded to Zn–O interaction at the tetrahedral site, whereas the bands around

300–450 cm⁻¹ were attributed to the stretching of Fe–O in the octahedral site [14].

The spectra of ZnE₁N, ZnE₃N, ZnE₅N, ZnE₁NK, ZnE₃NK, and ZnE₅NK at 414, 424, 416, 430, 430, and 434 cm⁻¹ respectively, correspond to the intrinsic stretching vibration of Fe–O at the octahedral position, whereas the other absorption bands at 546, 558, 546, 548, 550, and 560 cm⁻¹ correspond to the stretching of Zn–O at the tetrahedral position. The adsorption band shifted with the decrease of particle size and with the increase of temperature. The difference in the absorption region was probably due to the varying Zn–O bond distance in the ZnFe₂O₄ spinel structure. Besides, the spectrum also showed that the intensity of the calcined sample (Fig. 10b) was sharper than the uncalcined sample (Fig. 10a). This observation is probably due to the calcination process that formed a regular ferrite spinel structure. From the obtained spectrum bands, it can be concluded that the resulting sample is spinel ferrite. The peaks around 1400–1600 cm⁻¹ for the uncalcined sample indicated the presence of bending and stretching of C=O, C–O, OH, and COO⁻ derivatives of the secondary metabolites and other organic compounds contained in the Simbang Darah leaf extract [7].

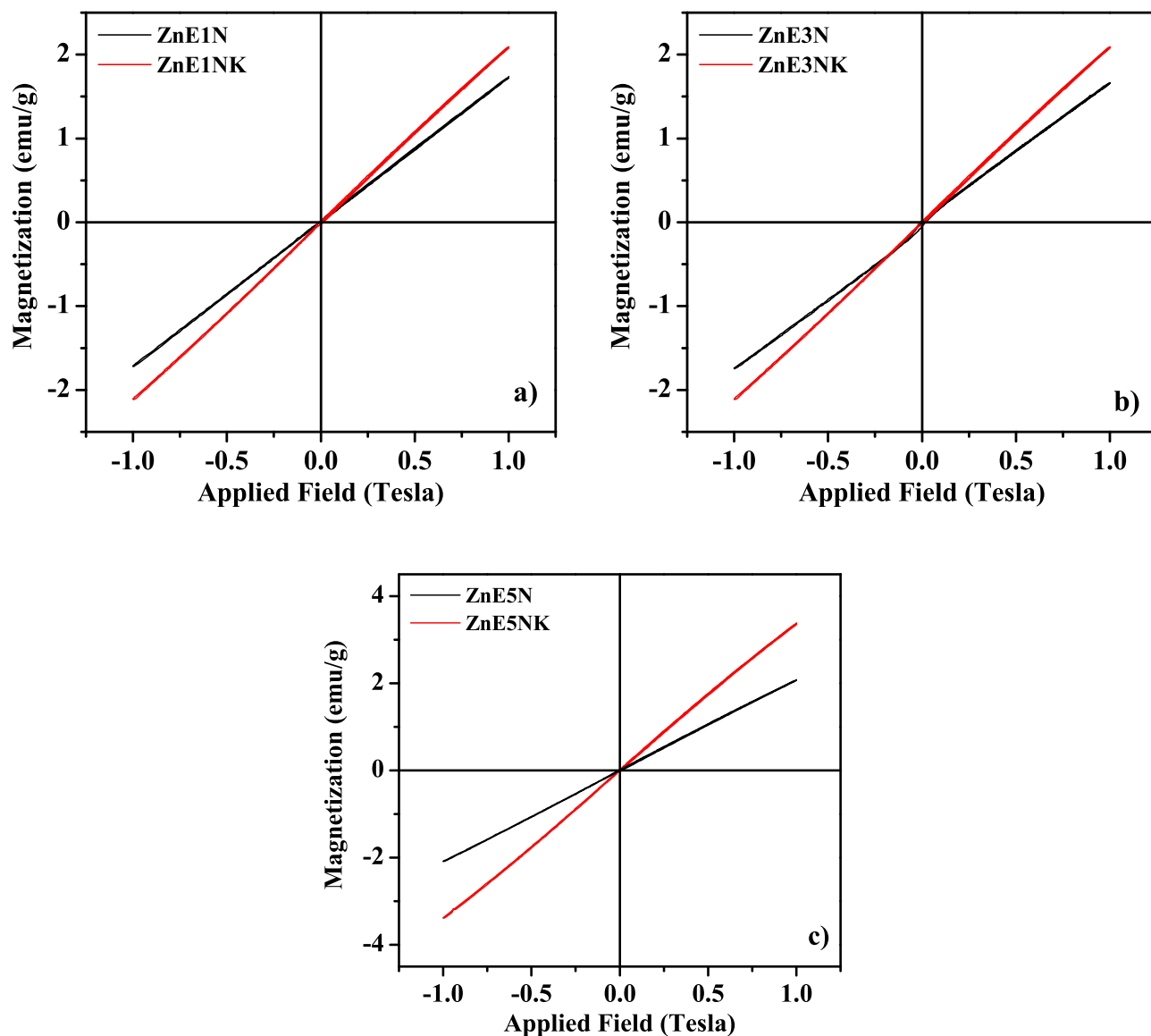


Fig. 9. Magnetic properties of samples (a) ZnE₁N and ZnE₁NK (b) ZnE₃N and ZnE₃NK, and (c) ZnE₅N and ZnE₅NK.

Table 2

Crystallite size, band gap, and magnetic behavior of Zn-ferrites before and after calcination.

Catalysts	Crystallite Size nm	Band gap eV	Magnetic saturation (Ms) (emu/g)	Magnetic remanent (Mr) (Mr)	Coercivity field (Hc) Tesla
ZnE ₁ N	7.2	2.08	1.69	0.006	0.006
ZnE ₃ N	6.8	2.11	1.74	0.026	0.011
ZnE ₅ N	6.2	2.12	2.08	0.014	0.004
ZnE ₁ NK	15.8	2.05	2.07	0.013	0.007
ZnE ₃ NK	16.9	2.11	2.11	0.011	0.006
ZnE ₅ NK	14.4	2.10	3.36	0.007	0.006

3.9. BET analysis

The nitrogen adsorption-desorption isotherms of the ZnE₁N sample was measured using the Brunauer-Emmett-Teller (BET) technique to investigate the specific surface area and porous structure of the ZnE₁N and ZnE₁NK (Fig. 11). The findings revealed the specific relation between the adsorbate's concentration and its adsorption degree with the

adsorbent surface [16]. According to IUPAC classification, the ZnE₁N and ZnE₁NK are type IV isotherms, characterized by their mesoporous structure [40].

The branch preceding the hysteresis loop corresponded to monolayer adsorption whereas the hysteresis loop is associated with capillary condensation in relatively coarse pores or the interstices between the particles of the zinc ferrite spinel. The increase in the adsorption branch with the sharp decline in the desorption branch observed at P/P₀ was greater than 0.6 due to the capillary condensation of N₂ into the mesoporous structure, indicating good homogeneity of the nanocomposite [41]. The specific surface area of samples obtained from the nitrogen adsorption-desorption measurement was 134.3 and 125.5 m²/g for ZnE₁N, and 114.28 and 110.27 m²/g for ZnE₁NK, respectively. The decreased surface area of ZnE₁NK after calcination may be attributed to the recrystallization of the zinc ferrite and subsequent increase in average crystallite size [16]. The total pore volume of ZnE₁N is 0.265 cc/g and 0.250 cc/g for ZnE₁NK. The samples' average pore diameter calculated using the Barrett-Joyner-Halenda equation was 1.69 and 1.71 nm for ZnE₁N and ZnE₁NK, respectively. The increased pore size after calcination may be due to the particles' rearrangement that led to the loss of the actual pores. Thus, the large surface area would

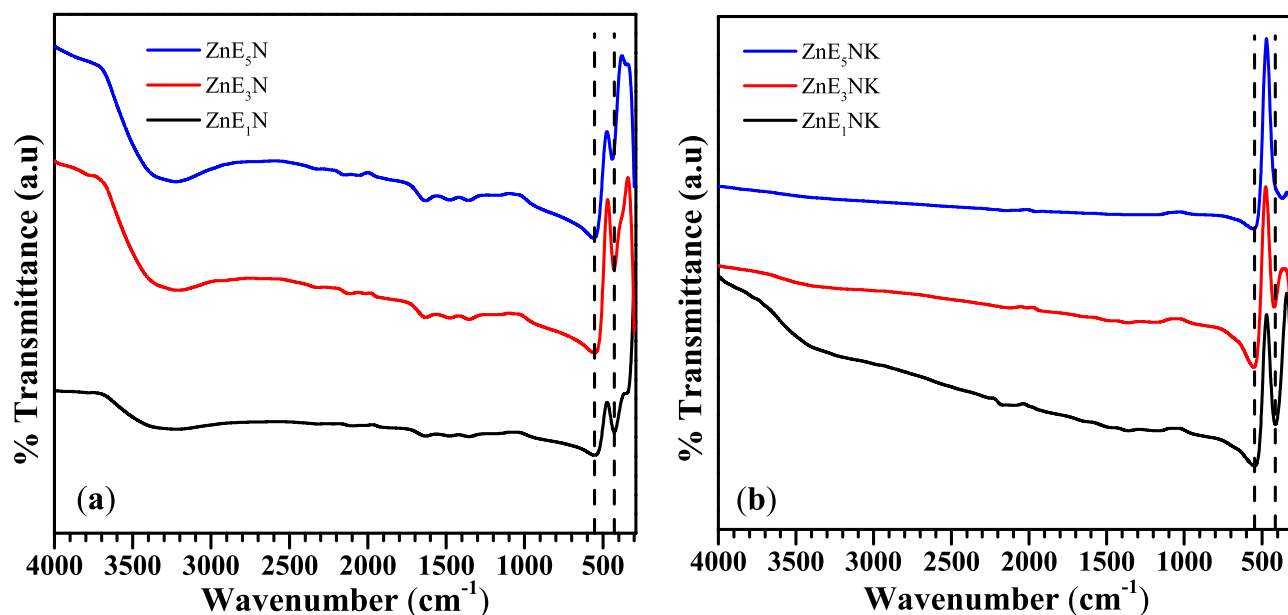


Fig. 10. FTIR spectrums of ZnFe₂O₄ before (a) and after calcination (b).

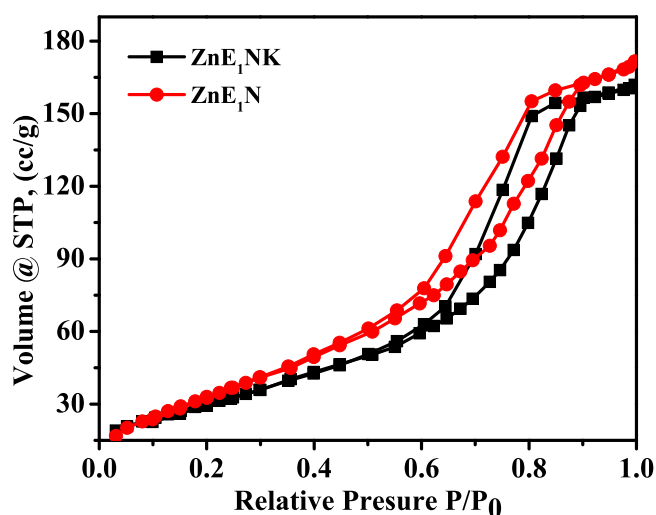


Fig. 11. Nitrogen adsorption-desorption isotherms of the ZnE₁N and ZnE₁NK.

make this material useful in photocatalytic processes.

3.10. Photocatalytic activity

Photocatalytic activity of the zinc ferrite prepared samples was determined based on the degradation of direct red 81 dyes using direct sunlight as a light source (Fig. 12). The experiment was carried out in triplicates. Sunlight is used for the photocatalytic process because it is an abundant, low-cost, and environmentally friendly, renewable source of clean energy. Fig. 12a shows the photocatalytic activity of all prepared samples on the degradation of direct red 81 dye under direct sunlight. The results showed that all catalysts have good activity against the degradation of direct red 81 dyes. The highest percentage of degradation was obtained using ZnE₁N as expected because of its smaller particle size and homogeneous morphology compared to other samples that contain more active sites to interact with the light to produce hydroxide radicals as illustrated in the electron images (SEM and TEM images). Hydroxyl radicals are known to be responsible for the photodegradation process of organic pollutants in the presence of natural sunlight.

The effect of dye concentration on the rate of degradation was determined by varying the concentration of direct red 81, as shown in Fig. 12b using ZnE₁N and ZnE₁NK as catalysts. The optimal concentration was obtained at 30 mg L⁻¹ with degradation percentage of 99.8% and 95.8% for 2 h using ZnE₁N and ZnE₁NK, respectively. Meanwhile, Fig. 12c shows the effect of irradiation time on the degradation percentage of direct red 81 dyes in the presence of ZnE₁N and ZnE₁NK. It was found that the degradation of dyes increased with irradiation time since the amount of OH· radicals formed increased with time. The OH· radicals were active groups that played a role in breaking down the dyes molecules into simpler compounds (ex: H₂O and CO₂) [42]. Furthermore, the maximum degradation percentage (99.66%) was obtained using ZnE₁N for 2 h under solar irradiation. Since ZnE₁N catalyst has higher dye decomposition efficiency than its calcined counterpart, all further experiments were performed using ZnE₁N.

An important property of photocatalysts is their recovery and repeated usage in catalytic processes. To test this characteristic, the ZnE₁N catalyst was repeatedly used in the photodegradation process of direct red 81 dyes under natural sunlight. In between each cycle, the catalysts were recovered via filtration, washed with distilled water, and dried at 105 °C. Fig. 12d shows the degradation percentage of direct red 81 dyes using ZnE₁N for four cycles which demonstrated that the catalyst remained fairly effective after being used for 4 cycles, indicating its stability and ability to be used repeatedly. Photodegradation of dyes/organic pollutants by different catalysts can be seen in Table 3.

The kinetics for photocatalysts are described in the Langmuir-Hinshelwood model, which can be expressed by $\ln(C_0/C_t) = kt$ when the dye concentration is relatively low (where C_0 is the initial concentration of dye, C_t is the concentration at time t and k is the apparent first-order rate constant). By plotting $\ln(C_0/C_t)$ vs irradiation time, t , k can be determined, which can be used as an assessment index for evaluating the photocatalytic efficiency of synthesized materials. Based on Fig. 12e, it was observed that the kinetic plot for catalysts was somewhat linear. Hence, the photodegradation reaction of direct red 81 dyes with ZnE₁N catalyst is of the first order with an r value of 0.985 and $k = 0.01204$ s⁻¹.

The primary mechanism of photocatalytic activity (Fig. 13) in the presence of ZnFe₂O₄ as a catalyst was initiated through the electrons transfer (e⁻) from the valence band (VB) to the conduction band (CB) if a certain amount of photon energy was absorbed by the electrons, leaving a hole (h⁺) in the VB. Then, CB's electrons reacted with O₂ in the water to form superoxide radical anions through a reduction reaction.

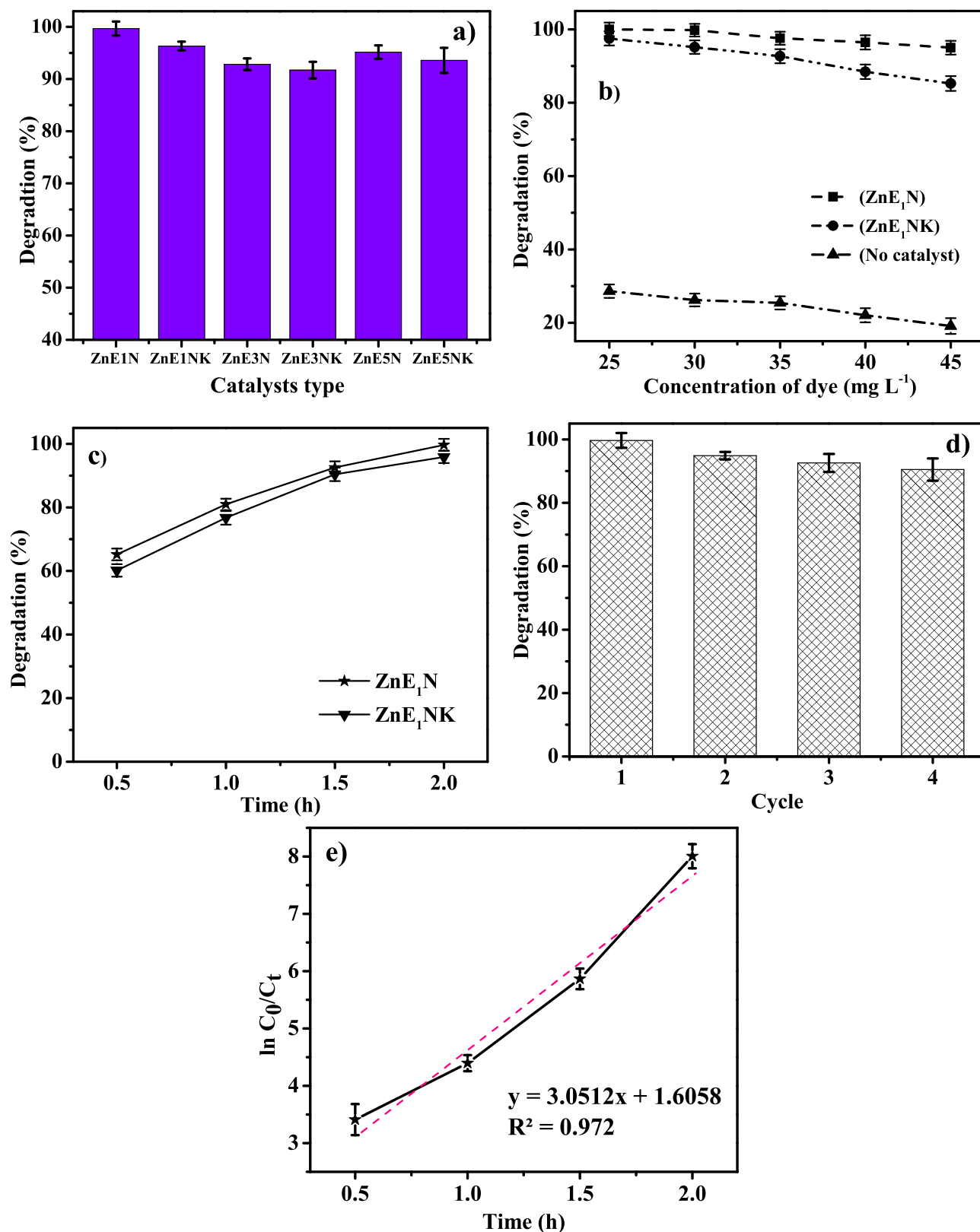


Fig. 12. Degradation percentage of the dye with various catalyst, dye concentrations, and irradiation time (a-c), photocatalytic stability determination (d), and reaction kinetics of the photocatalytic process (e).

Superoxide radicals then underwent protonation to form H_2O_2 , which then dissociated to form $OH\cdot$ radicals. This radical avoided the recombination of e^-/h^+ pairs and participated in the oxidation process. On the other hand, OH^- derived from the decomposition of water molecules

reacted with the hole (h^+) in VB through oxidation reactions, forming $OH\cdot$ radicals. Furthermore, $OH\cdot$ radicals attacked the organic pollutants or dyes to form unstable intermediates and broke them down into simple molecules, i.e., water, and carbon dioxide gas [46].

Table 3
Comparing photodegradation of dyes/organic pollutants by different catalysts.

No	Catalyst	Synthesis method	Name of dyes/ organic pollutant	% of degradation	Ref.
1.	ZnFe ₂ O ₄	Green synthesis	Direct Red 81	99.66	This work
2.	ZnFe ₂ O ₄	Co-precipitation	Methylene Blue	99	[11]
3.	ZnFe ₂ O ₄	Combustion route	Rhodamine B, Methylene Blue	98	[14]
				95	
4.	ZnFe ₂ O ₄	Co-precipitation	Acid Blue 113	92	[16]
5.	ZnFe ₂ O ₄	Green method	Methylene Blue	99.6	[21]
			Evan Blue	89	
6.	ZnFe ₂ O ₄	Green synthesis	Tetracycline	80	[34]
7.	ZnFe ₂ O ₄	Combustion	Congo Red	95	[9]
			Rhodamine B	93.6	
8.	ZnFe ₂ O ₄	Hydrothermal	Methylene blue	90	[43]
9.	NiFe ₂ O ₄ /natural mineral	Microwave hydrothermal	Sodium dodecyl benzene sulfonate	100	[13]
10.	ZnFe ₂ O ₄ / Polyaniline	Co-precipitation	Rhodamine B	85	[10]
11.	ZnO-CoFe ₂ O ₄	Green method	Direct Yellow	95	[28]
12.	MnFe ₂ O ₄	Green method	Direct Red 81	56.5	[30]
13.	SnFe ₂ O ₄ /Polypyrrole	Sonication	Tartrazine	100	[44]
14.	NiFe ₂ O ₄	Co-precipitation	Methyl Orange	72.66	[45]

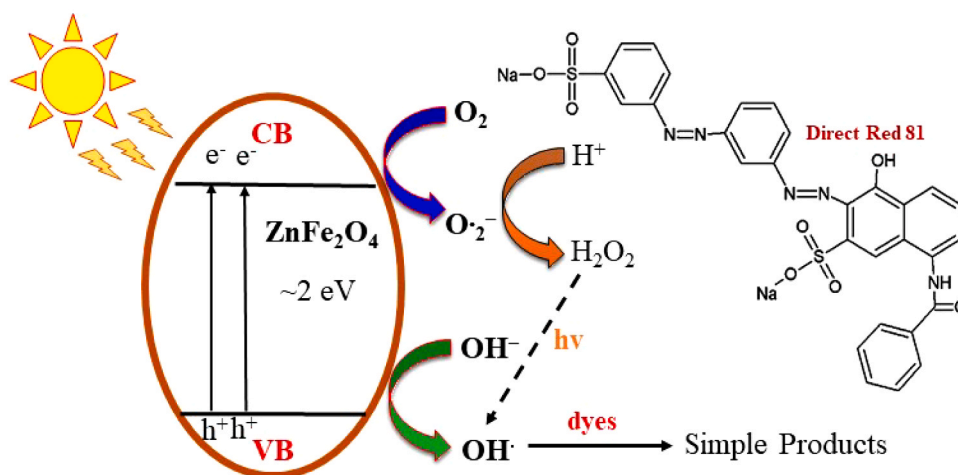


Fig. 13. The proposed photocatalytic mechanism of the direct red 81 using ZnFe₂O₄ as a catalyst.

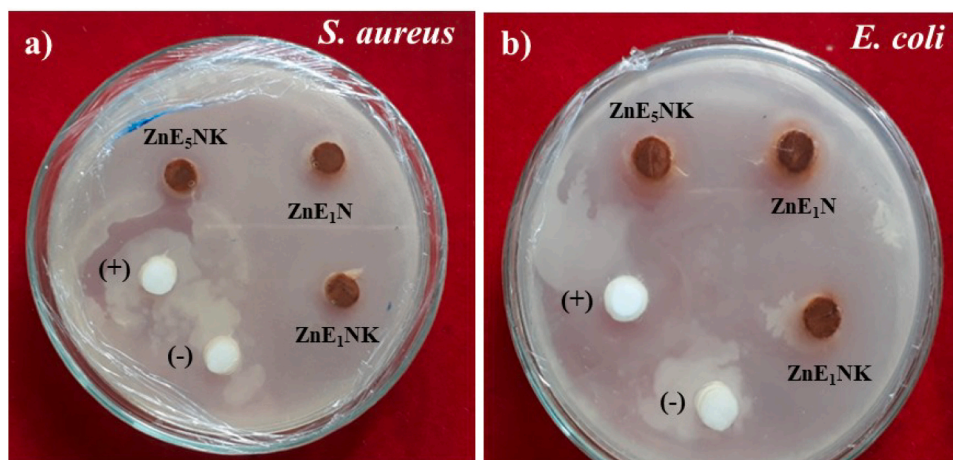


Fig. 14. Antibacterial activity of ZnFe₂O₄ on *S. aureus* (a) and *E. coli* (b).

3.11. Antibacterial activity

The antibacterial assay for ZnE₁N, ZnE₁NK, and ZnE₅NK samples was conducted using Gram-positive (*S. aureus*) and Gram-negative (*E. coli*) as pathogens. The results are shown in Fig. 14. ZnE₁N, ZnE₁NK, and ZnE₅NK ferrite samples showed positive antibacterial activity against *S. aureus* with an inhibition zone of 10.9, 10, and 9.4 mm in respectively, whereas for *E. coli* were 9.6, 4.9, and 7.5 mm, respectively. Amoxicillin and water were used as a positive and negative control in this experiment. The bacterial activity of zinc ferrite depends on the size, morphology, chemical molecule diffusion ability, and the discharge of metal ions. In addition, the surface area is crucial in the elevated and promising activity of ZnFe₂O₄ nanoparticles against all the tested pathogenic microbes. There are many reasonable mechanisms for the antimicrobial action of ZnFe₂O₄ nanoparticles, including radical groups generated through the redox reactions during the photocatalytic process attack the bacteria's cell membrane components and inhibit the growth of these microorganisms [47].

4. Conclusion

The ferrite spinel of ZnFe₂O₄ nanostructures has been successfully synthesized using Simbang Darah extract as a capping agent via the hydrothermal method. Characterization using several instruments showed that the samples were in the form of homogeneous spherical granules. The synthesized zinc ferrite nanoparticles exhibited paramagnetic and absorbent behavior under the visible light with a band gap energy of ~ 2 eV. The ZnFe₂O₄ nanoparticles showed effective photodegradation for direct red 81 at 99.66% for 2 h under solar light irradiation. Moreover, these nanoparticles demonstrated antibacterial activities against *S. aureus* and *E. coli*. Therefore, it can be concluded that Simbang Darah extract provided a good yield of ferrite nanoparticles with desirable properties. Thus, it can be used to synthesize other materials in nanoscale.

CRedit authorship contribution statement

Rahmayeni: Conceptualization, Methodology, Validation, Writing - Original Draft, **Rike Febrialita:** Investigation, Visualization, **Yeni Stiadi:** Writing - Original Draft, **Yulia Eka Putri:** Visualization, Validation, **Nofrijon Sofyan:** Writing - Review & Editing, **Zulhadjri:** Writing - Review & Editing.

Declaration of Competing Interest

The authors declare that they have no known competing financial interests or personal relationships that could have appeared to influence the work reported in this paper.

Acknowledgment

This work was funded by DRPM, Kementerian Pendidikan dan Kebudayaan of the Republic of Indonesia under Penelitian Dasar Kompetitif [grant contract number: T/26/UN.16.17/PT.01.03/AMD/PD-Material Maju/2020, 10 Maret 2020].

References

- R. Rameshbabu, R. Ramesh, S. Kanagesan, A. Karthigeyan, S. Ponnusamy, Synthesis of superparamagnetic ZnFe₂O₄ nanoparticle by surfactant-assisted hydrothermal method, *J. Mater. Sci. Mater. Electron.* 24 (2013) 4279–4283, <https://doi.org/10.1007/s10854-013-1397-6>.
- V. Seetha Rama Raju, Synthesis of non-stoichiometric zinc ferrite for electromagnetic wave absorber applications, *Mater. Sci. Eng. B Solid-State Mater. Adv. Technol.* 224 (2017) 88–92, <https://doi.org/10.1016/j.mseb.2017.07.012>.
- S.M. Hoque, M.S. Hossain, S. Choudhury, S. Akhter, F. Hyder, Synthesis and characterization of ZnFe₂O₄ nanoparticles and its biomedical applications, *Mater. Lett.* 162 (2016) 60–63, <https://doi.org/10.1016/j.matlet.2015.09.066>.
- F. Martinez-Julian, A. Guerrero, M. Haro, J. Bisquert, D. Bresser, E. Paillard, S. Passerini, G. Garcia-Belmonte, Probing lithiation kinetics of carbon-coated ZnFe₂O₄ nanoparticle battery anodes, *J. Phys. Chem. C* 118 (2014) 6069–6076, <https://doi.org/10.1021/jp412641v>.
- K. Wu, J. Li, C. Zhang, Zinc ferrite based gas sensors: a review, *Ceram. Int.* 45 (2019) 11143–11157, <https://doi.org/10.1016/j.ceramint.2019.03.086>.
- S.V. Bangale, Nanostructured ZnCo₂O₄ thick film as an ethanol sensor, *Int. J. Smart Sens. Intell. Syst.* 7 (2014) 178–195, <https://doi.org/10.21307/ijssis-2017-651>.
- S.O. Aisida, P.A. Akpa, I. Ahmad, M. Maaza, F.I. Ezema, Influence of PVA, PVP and PEG doping on the optical, structural, morphological and magnetic properties of zinc ferrite nanoparticles produced by thermal method, *Phys. B Condens. Matter* 571 (2019) 130–136, <https://doi.org/10.1016/j.physb.2019.07.001>.
- M. Madhukara Naik, H.S. Bhojya Naik, G. Nagaraju, M. Vinuth, K. Vinu, R. Viswanath, Green synthesis of zinc doped cobalt ferrite nanoparticles: structural, optical, photocatalytic and antibacterial studies, *Nano-Struct. Nano-Objects* 19 (2019), 100322, <https://doi.org/10.1016/j.nanos.2019.100322>.
- A. Behera, D. Kandi, S.M. Majhi, S. Marthia, K. Parida, Facile synthesis of ZnFe₂O₄ photocatalysts for decolorization of organic dyes under solar irradiation, *Beilstein J. Nanotechnol.* 9 (2018) 436–446, <https://doi.org/10.3762/bjnano.9.42>.
- N.B. Singh Rachna, A. Agarwal, Preparation, characterization, properties and applications of nano zinc ferrite, *Mater. Today Proc.* 5 (2018) 9148–9155, <https://doi.org/10.1016/j.matpr.2017.10.035>.
- N.G. Yadav, L.S. Chaudhary, P.A. Sakhare, T.D. Dongale, P.S. Patil, A.D. Sheikh, Impact of collected sunlight on ZnFe₂O₄ nanoparticles for photocatalytic application, *J. Colloid Interface Sci.* 527 (2018) 289–297, <https://doi.org/10.1016/j.jcis.2018.05.051>.
- H. Yang, X. Bai, P. Hao, J. Tian, Y. Bo, X. Wang, H. Liu, A simple gas sensor based on zinc ferrite hollow spheres: highly sensitivity, excellent selectivity and long-term stability, *Sens. Actuators B Chem.* 280 (2019) 34–40, <https://doi.org/10.1016/j.snb.2018.10.036>.
- W. Shen, L. Zhang, B. Zhao, Y. Du, X. Zhou, Growth mechanism of octahedral like nickel ferrite crystals prepared by modified hydrothermal method and morphology dependent magnetic performance, *Ceram. Int.* 44 (2018) 9809–9815, <https://doi.org/10.1016/j.ceramint.2018.02.219>.
- S.B. Patil, H.S. Bhojya Naik, G. Nagaraju, R. Viswanath, S.K. Rashmi, M. Vijay Kumar, Sugarcane juice mediated eco-friendly synthesis of visible light active zinc ferrite nanoparticles: application to degradation of mixed dyes and antibacterial activities, *Mater. Chem. Phys.* 212 (2018) 351–362, <https://doi.org/10.1016/j.matchemphys.2018.03.038>.
- D.O. Okoroh, J. Ozuomba, S.O. Aisida, P.U. Asogwa, Thermal treated synthesis and characterization of polyethylene glycol (PEG) mediated zinc ferrite nanoparticles, *Surf. Interfaces* 16 (2019) 127–131, <https://doi.org/10.1016/j.surfin.2019.05.004>.
- S. Mandal, S. Natarajan, A. Tamilselvi, S. Mayadevi, Photocatalytic and antimicrobial activities of zinc ferrite nanoparticles synthesized through soft chemical route: a magnetically recyclable catalyst for water/wastewater treatment, *J. Environ. Chem. Eng.* 4 (2016) 2706–2712, <https://doi.org/10.1016/j.jece.2016.05.020>.
- M. Sriramulu, D. Shukla, S. Sumathi, Aegle marmelos leaves extract mediated synthesis of zinc ferrite: antibacterial activity and drug delivery, *Mater. Res. Express* 5 (2018) 1–9, <https://doi.org/10.1088/2053-1591/aad888>.
- P. Laokul, V. Amornkitbamrung, S. Seraphin, S. Maensiri, Characterization and magnetic properties of nanocrystalline CuFe₂O₄, NiFe₂O₄, ZnFe₂O₄ powders prepared by the Aloe vera extract solution, *Curr. Appl. Phys.* 11 (2011) 101–108, <https://doi.org/10.1016/j.cap.2010.06.027>.
- K. Kombariah, J.J. Vijaya, L.J. Kennedy, M. Bououdina, K. Kaviyarasu, R. J. Ramalingam, M.A. Munusamy, A. AlArfaj, Effect of Cd²⁺ concentration on ZnFe₂O₄ nanoparticles on the structural, optical and magnetic properties, *Optik* 135 (2017) 190–199, <https://doi.org/10.1016/j.ijleo.2017.01.066>.
- N. Matinise, K. Kaviyarasu, N. Mongwaketsi, S. Khamlich, L. Kotsedi, N. Mayedwa, M. Maaza, Green synthesis of novel zinc iron oxide (ZnFe₂O₄) nanocomposite via Moringa oleifera natural extract for electrochemical applications, *Appl. Surf. Sci.* 446 (2018) 66–73, <https://doi.org/10.1016/j.apsusc.2018.02.187>.
- M. Madhukara Naik, H.S. Bhojya Naik, G. Nagaraju, M. Vinuth, H. Raja Naika, K. Vinu, Green synthesis of zinc ferrite nanoparticles in Limonia acidissima juice: characterization and their application as photocatalytic and antibacterial activities, *Microchem. J.* 146 (2019) 1227–1235, <https://doi.org/10.1016/j.microc.2019.02.059>.
- S.N. Ijioma, K.K. Igwe, O.N. Nwakudu, A.J. Madubuike, N.K. Achi, Preliminary evaluation of phytochemicals in Iresine herbistii ethanol leaf extract using gas chromatography-mass spectrometry analysis, *J. Environ. Life Sci.* 2 (2017) 21–28.
- G. Nencini, F. Cavallo, G. Bruni, A. Capasso, V. De Feo, L. De Martino, G. Giorgi, L. Micheli, Affinity of Iresine herbistii and Brugmansia arborea extracts on different cerebral receptors, *J. Ethnopharmacol.* 105 (2006) 352–357, <https://doi.org/10.1016/j.jep.2005.11.022>.
- Y. Cai, M. Sun, H. Corke, Identification and distribution of simple and acylated betacyanins in the Amaranthaceae, *J. Agric. Food Chem.* 49 (2001) 1971–1978, <https://doi.org/10.1021/jf000963h>.
- M. Valentová, R. Marek, E. Švajdlenka, R. Kubínová, V. Suchý, A new isoflavonone from Iresine herbistii, *Fitoterapia* 82 (2011) 272–275, <https://doi.org/10.1016/j.fitote.2010.10.010>.
- E. Walger, N. Marlin, F. Molton, G. Mortha, Study of the direct red 81 dye/copper (II)-phenanthroline system, *Molecules* 23 (2018) 1–23, <https://doi.org/10.3390/molecules23020242>.
- S. Khamparia, D. Jaspal, Adsorptive removal of Direct Red 81 dye from aqueous solution onto Argemone mexicana, *Sustain. Environ. Res.* 26 (2016) 117–123, <https://doi.org/10.1016/j.serj.2016.04.002>.

- [28] Rahmayeni, A. Alfina, Y. Stiadi, H.J. Lee, Zulhadjri, Green synthesis and characterization of ZnO-CoFe₂O₄ semiconductor photocatalysts prepared using rambutan (*Nephelium lappaceum* L.) peel extract, *Mater. Res.* 22 (2019) 2–11, <https://doi.org/10.1590/1980-5373-MR-2019-0228>.
- [29] B.A. Hunter, Rietica - A Visual Rietveld Program, Australian Nuclear Science and Technology Organisation, Australia, 2000.
- [30] R. Rahmayeni, Y. Oktavia, Y. Stiadi, S. Arief, Z. Zulhadjri, Spinel ferrite of MnFe₂O₄ synthesized in Piper betle Linn extract media and its application as photocatalysts and antibacterial, *J. Dispers. Sci. Technol.* 42 (2021) 465–474, <https://doi.org/10.1080/01932691.2020.1721011>.
- [31] K. Ashwini, H. Rajanaika, K.S. Anantharaju, H. Nagabhushanad, P. Adinarayana Reddy, K. Shetty, K.R. Vishnu Mahesh, Synthesis and characterization of as-formed and calcined MnFe₂O₄ nanoparticles: a comparative study of their antibacterial activities, *Mater. Today Proc.* 4 (2017) 11902–11909, <https://doi.org/10.1016/j.matpr.2017.09.110>.
- [32] N. Masunga, O.K. Mmesili, K.K. Kefeni, B.B. Mamba, Recent advances in copper ferrite nanoparticles and nanocomposites synthesis, magnetic properties and application in water treatment: review, *J. Environ. Chem. Eng.* 7 (2019), 103179, <https://doi.org/10.1016/j.jece.2019.103179>.
- [33] S. Rohilla Seema, Rietveld refinement and structural characterization of powder ZnFe₂O₄ synthesized through co-precipitation method, *AIP Conf. Proc.* 2142 (2019) 2–7, <https://doi.org/10.1063/1.5122522>.
- [34] M.I. Din, S. Jabbar, J. Najeeb, R. Khalid, T. Ghaffar, M. Arshad, S.A. Khan, S. Ali, Green synthesis of zinc ferrite nanoparticles for photocatalysis of methylene blue, *Int. J. Phytoremediat.* 0 (2020) 1–8, <https://doi.org/10.1080/15226514.2020.1781783>.
- [35] S.K. Rashmi, H.S. Bhojya Naik, H. Jayadevappa, R. Viswanath, S.B. Patil, M. Madhukara Naik, Solar light responsive Sm-Zn ferrite nanoparticle as efficient photocatalyst, *Mater. Sci. Eng. B Solid-State Mater. Adv. Technol.* 225 (2017) 86–97, <https://doi.org/10.1016/j.mseb.2017.08.012>.
- [36] K. Laohhasurayotin, S. Pookboonmee, D. Viboonratanasri, Preparation of magnetic photocatalyst nanoparticles-TiO₂/SiO₂/Mn-Zn ferrite and its photocatalytic activity influenced by silica interlayer, *Mater. Res. Bull.* 47 (2012) 1500–1507, <https://doi.org/10.1016/j.materresbull.2012.02.030>.
- [37] Y. Cao, X. Lei, Q. Chen, C. Kang, W. Li, B. Liu, Enhanced photocatalytic degradation of tetracycline hydrochloride by novel porous hollow cube ZnFe₂O₄, *J. Photochem. Photobiol. A Chem.* 364 (2018) 794–800, <https://doi.org/10.1016/j.jphotochem.2018.07.023>.
- [38] R.S. Yadav, I. Kuřitka, J. Vilcakova, P. Urbánek, M. Machovsky, M. Masař, M. Holec, Structural, magnetic, optical, dielectric, electrical and modulus spectroscopic characteristics of ZnFe₂O₄ spinel ferrite nanoparticles synthesized via honey-mediated sol-gel combustion method, *J. Phys. Chem. Solids* 110 (2017) 87–99, <https://doi.org/10.1016/j.jpcs.2017.05.029>.
- [39] K. Kombaiah, J.J. Vijaya, L.J. Kennedy, M. Bououdina, Studies on the microwave-assisted and conventional combustion synthesis of Hibiscus rosa-sinensis plant extract-based ZnFe₂O₄ nanoparticles and their optical and magnetic properties, *Ceram. Int.* 42 (2016) 2741–2749, <https://doi.org/10.1016/j.ceramint.2015.11.003>.
- [40] L. Han, X. Zhou, L. Wan, Y. Deng, S. Zhan, Synthesis of ZnFe₂O₄ nanoplates by succinic acid-assisted hydrothermal route and their photocatalytic degradation of rhodamine B under visible light, *J. Environ. Chem. Eng.* 2 (2014) 123–130, <https://doi.org/10.1016/j.jece.2013.11.031>.
- [41] G. Kenanakis, Z. Giannakoudakis, D. Vernardou, C. Savvakis, N. Katsarakis, Photocatalytic degradation of stearic acid by ZnO thin films and nanostructures deposited by different chemical routes, *Catal. Today* 151 (2010) 34–38, <https://doi.org/10.1016/j.cattod.2010.02.054>.
- [42] S. Meena, L. Renuka, K.S. Anantharaju, Y.S. Vidya, H.P. Nagaswarupa, S. C. Prashantha, H. Nagabhushana, Optical, electrochemical and photocatalytic properties of sunlight driven Cu doped manganese ferrite synthesized by solution combustion synthesis, *Mater. Today Proc.* 4 (2017) 11773–11781, <https://doi.org/10.1016/j.matpr.2017.09.094>.
- [43] A. Arimi, L. Megatiff, L.I. Granone, R. Dillert, D.W. Bahnemann, Visible-light photocatalytic activity of zinc ferrites, *J. Photochem. Photobiol. A Chem.* 366 (2018) 118–126, <https://doi.org/10.1016/j.jphotochem.2018.03.014>.
- [44] J. Leichtweis, S. Silvestri, Y. Vieira, T.A. de Lima Burgo, E.L. Foletto, A novel tin ferrite/polymer composite use in photo-Fenton reactions, *Int. J. Environ. Sci. Technol.* (2020), <https://doi.org/10.1007/s13762-020-02944-1>.
- [45] S. Sendhilnathan Hirthna, P.I. Rajan, T. Adinaveen, Synthesis and Characterization of NiFe₂O₄ nanoparticles for the enhancement of direct sunlight photocatalytic degradation of methyl orange, *J. Supercond. Nov. Magn.* 31 (2018) 3315–3322, <https://doi.org/10.1007/s10948-018-4601-3>.
- [46] P. Chand Sukriti, V. Singh, D. Kumar, Rapid, visible-light-driven photocatalytic degradation using Ce-doped ZnO nanocatalysts, *Vacuum* 178 (2020), 109364, <https://doi.org/10.1016/j.vacuum.2020.109364>.
- [47] C. Regmi, B. Joshi, S.K. Ray, G. Gyawali, R.P. Pandey, Understanding mechanism of photocatalytic microbial decontamination of environmental wastewater, *Front. Chem.* 6 (2018) 1–6, <https://doi.org/10.3389/fchem.2018.00033>.